Contact analysis of a flexible bladed-rotor

Nicolas Lesaffre, Jean-Jacques Sinou, Fabrice Thouverez

Contact Analysis of a Flexible Bladed-Rotor

N. Lesaffre, J-J. Sinou and F. Thouverez

Ecole Centrale de Lyon
Laboratoire de Tribologie et Dynamique des Systèmes, UMR CNRS 5513
36 avenue Guy de Collongue
69134 Ecully Cedex, FRANCE

Abstract

This paper presents a model of fully flexible bladed rotor developed in the rotating frame. An energetic method is used to obtain the matrix equations of the dynamic behaviour of the system. The gyroscopic effects as well as the spin softening effects and the centrifugal stiffening effects, taken into account through a pre-stressed potential, are included in the model. In the rotating frame, the eigenvalues' imaginary parts of the latter matrix equation give the Campbell diagram of the system and its stability can be analysed through its associated eigenvalues' real parts. The turbo machine casing is also modelled by an elastic ring in the rotating frame through an energetic method. Thus, the contact problem between the rotor and the stator can be treated as a static problem. Prior to the study of the complete problem of contact between the flexible blades of the rotor and the flexible casing, a simple model of an elastic ring having only one mode shape, excited by rotating loads is developed in the rotating frame too, in order to underline divergence instabilities and mode couplings. Then, the real complex problem of contact between the blades and the casing, without rubbing, is studied. The stable balanced static contact configurations of the structure are found as function of the rotational speed of the rotor. Finally, the results are compared to these of the simple model of rotating spring-masses on an elastic ring.

Keywords

Rotor dynamics, flexible bladed-rotor, stability analysis, Campbell diagram, rotor/stator contacts, rotating loads.

I. Introduction

Nowadays, more than ever, turbo machinery designers seek for increase the efficiency of their machine what could result in a loss of weight and a decrease in fuel consumption. The efficiency of turbo-generators depends strongly on the clearance between the rotating and stationary parts (Song and Martinez-Sanchez, 1997-a, Song and Martinez-Sanchez, 1997-b, Childs, 1993, Ehrich, 1992, Yamamoto and Ishida, 2001): the wider the clearance, the less efficient the machine. Hence it is desirable to reduce the clearance by as much as possible. Unfortunately, it cannot be reduced below a certain minimum level due to uncertainties in the dynamics, fluid dynamics (Muszynska and Bently, 1996, Ehrich, 1993), thermal loads (Goldman and Muszynska, 1995), machining tolerances and material properties (Maozhong, et al., 2002, Marscher, 1980). The more accurately these parameters are known, the smaller the clearance that can be made. However, reduced clearances increase the possibility of violent contacts between rotor and stator. Under certain operating conditions, depending for instance on the dynamic properties of the rotor or/and the stator and on the rotational speed,

the contacts may lead to an unstable rotor-stator system (Feng and Zhang, 2002, Edwards et al., 1999).
A common interest of the rotating-machinery industry is to better understand the dynamic behaviour of rotating structures and in particular that of flexible bladed-rotors whose dynamic behaviour differs from those usually studied in rotor-dynamics especially because of the dynamics of the flexible blades that can lead to instabilities (Crandall and Dugundji, 1981, Genta, 2003). The study of such structures is quite complex and must be performed using numerical models (Gmür, 1997, Lalanne and Ferraris, 1990). To obtain a closed form solution suitable for stability analysis, it is possible to resort to simplified models (Sinha, 2004, Al-Bedoor and Al-Qaisia, 2005, Turhan and Bulut, 2005).
It is fundamental for turbo machinery industries to understand the leading phenomenon in case of contacts between the blades of the rotor and the casing and some researches have been recently investigated (Schmiechen, 1997, Arnoult, 1998, Legrand, 2005).
This paper presents firstly a simplified model of a flexible fully-bladed rotor constructed in the rotating frame by using an energetic approach and taking into account the basic effects of rotating machines. In a second part, an elastic ring having only one mode shape is modelled also in the rotating frame by using an energetic method. Its behaviour when excited by rotating loads is studied. Finally, the contact problem of the blades of the rotor with a casing modelled by a flexible ring is investigated. The results and the phenomenon underlined are compared to the latter ones.

II. Model formulation

The rotor considered in this study is shown on Fig. 1. The model is inspired from an existing model by Sinha (Sinha, 2004) but developed in the rotating frame by using an energetic method. The rotor is composed of a shaft modelled by an Euler-Bernoulli beam, connected to a rigid disk modelled by a concentrated mass with rotational inertia. This shaft is set on bearings at multiple locations. On the rigid disk is clamped a full set of flexible blades also modelled by Euler-Bernoulli beams.
In the rotating frame, two degrees of freedom are considered for the shaft: two orthogonal translations $u(z,t)$ and $\upsilon(z,t)$ in the disk's plane (see Fig. 2), and one degree of freedom for each blade defining its deflection $\eta_j(s,t)$.
A Rayleigh-Ritz approximation is used to express the degrees of freedom of these different parts. Thus, they are expressed by a sum of shape functions multiplied by time-dependent coefficients:

$$u(z,t) = U_o(t) + \sum_{m=1}^{m_{tot}} U_m(t) W_m(z) \tag{1}$$

$$\upsilon(z,t) = V_o(t) + \sum_{m=1}^{m_{tot}} V_m(t) W_m(z) \tag{2}$$

$$\eta_j(s,t) = \sum_{n=1}^{n_{tot}} (X_n(t))_j (Y_n(s))_j \tag{3}$$

where z is the axis of the shaft and s, the axis along the blade. In these expressions, $U_o(t)$ and $V_o(t)$ are rigid-body translations of the shaft. m_{tot} and n_{tot} are the number of modes considered to express its motion and the flexure of the j^{th} blade respectively. In this Rayleigh-Ritz approach, the shape functions have only to verify the geometric boundary conditions of the problem. Due to the fact that all blades are clamped in the rigid disk, the shape functions of these latter ones must verify $Y_n(0)=0$ and $Y_n'(0)=0$, where prime denotes

differentiation versus space coordinates. Thus, the chosen expression for the shape function of the blade deflection is:

$$Y_n(s) = a_n s + \sin(\beta_n s) \tag{4}$$

with $\beta_n=(2n-1)\pi/(2L)$, and $a_n = -\beta_n$. Concerning the shaft, since it is supported by bearings, its shape function has no geometric boundary conditions to verify and its chosen expression is:

$$W_m(z)=1-\cos(\alpha_m z) \tag{5}$$

with $\alpha_m=(2m-1)\pi/(2l)$. However, it could be noticed that these functions verify $W_m(0)=0$ and $W_m'(0)=0$ thus no motion is permitted at the right end of the shaft (i.e. at z = 0).

Since an energetic method is used to develop this model, energies and potentials have to be defined for the shaft and for the blades as well. Thus, the kinetic energy T_{blade} of the j^{th} blade, located at an angle $\varphi_j=\frac{2\pi j}{N_{tot}}$ in this frame (as indicated in Fig. 2) where N_{tot} is the total number of blades, can be fully expressed by the following relation:

$$T_{blade} = \int_0^L \frac{1}{2}\rho_b S_b \vec{V}^2_{S/R_0}(G)ds + \int_0^L \frac{1}{2}\vec{\Omega}^T_{S/R_0}\mathbf{I}\vec{\Omega}_{S/R_0}ds \tag{6}$$

where ρ_b and S_b are the density and the area of a blade cross section respectively. $\vec{V}_{S/R0}(G)$, $\vec{\Omega}_{S/R0}$ and $\mathbf{I}$ are the speed, the rotation of the mass center of a blade cross section (in relation to the fixed frame) and its inertia matrix, defined in its inertial frame. It may be noticed that the complete expression of the kinetic energy should be considered because in certain extreme geometric conditions, an approached kinetic energy can lead to unrealistic instabilities of the rotor.

The potential energy $v_{\text{int}blade}$ associated with the elastic deformation of the blade:

$$v_{\text{int}blade} = \frac{1}{2}\int_0^L E_b I_b(\eta''(s,t))^2 ds \tag{7}$$

where E_b and I_b are the elastic Young's modulus of the blade material and the blade area moment of inertia for flexure respectively, is defined, as well as a function of dissipation F_{dblade} associated with the internal damping (viscous damping with coefficient η_b) of the j^{th} blade:

$$F_{dblade} = \frac{1}{2}\int_0^L \eta_b E_b I_b(\dot{\eta}''(s,t))^2 ds \tag{8}$$

Next, a pre-stress potential taking into account the centrifugal stiffening effects is defined by:

$$v_{g_{blade}} = \frac{1}{2}\int_0^L \rho_b S_b \Omega^2 \left[\frac{R^2-(s+r)^2}{2}\right]\eta'^2(s,t)ds \tag{9}$$

In the same way, the kinetic energy T_{shaft} (Lesaffre et al., in press), the potential energy $v_{\text{int}shaft}$ associated with the elastic deformation of the shaft:

$$v_{\text{int}_{shaft}} = \frac{1}{2}\int_0^l E_s I_s(u''^2(z,t) + \upsilon''^2(z,t))dz \tag{10}$$

where E_s and I_s are the elastic Young's modulus of the shaft material and the shaft area moment of inertia for flexure respectively, are defined, as well as a function of dissipation F_{dshaft} associated with the internal damping (viscous damping with coefficient η_s) of the shaft:

$$F_{d_{shaft}} = \frac{1}{2}\int_0^l \eta_s E_s I_s(\dot{u}''^2(z,t) + \dot{\upsilon}''^2(z,t))dz \tag{11}$$

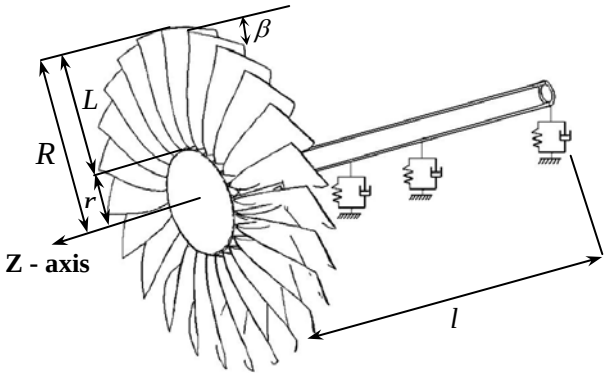

Figure 1 Model of flexible bladed-rotor (Sinha, 2004)

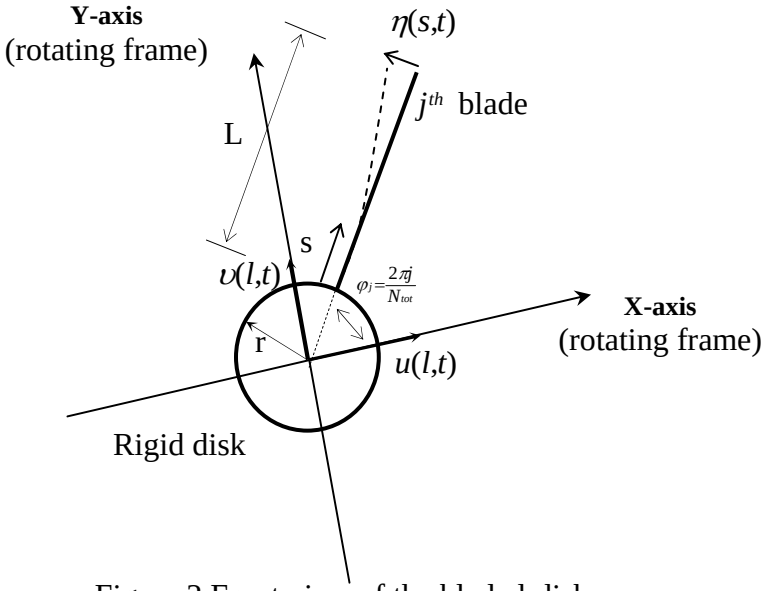

Figure 2 Front view of the bladed-disk

The bearings are introduced through a potential $v_{bearings}$ and a function of dissipation $F_{dbearings}$ associated with their damping (Lesaffre et al., in press).

Then, Lagrange's equations are used to obtain the system of equations of the dynamic behaviour of the full flexible bladed-rotor. This system of equations can be written under the following form:

$$\mathbf{M}_{rotor}\ddot{\mathbf{X}}_{rotor} + \left(\mathbf{D}_{rotor} + \mathbf{G}_{rotor}\right)\dot{\mathbf{X}}_{rotor} + \left(\mathbf{K}_{rotor} + \mathbf{K}_{geom_{rotor}} + \mathbf{N}_{rotor}\right)\mathbf{X}_{rotor} = \mathbf{0} \quad (12)$$

where $\mathbf{M}_{rotor}$, $\mathbf{D}_{rotor}$, $\mathbf{G}_{rotor}$, $\mathbf{K}_{rotor}$, $\mathbf{K}_{geom_{rotor}}$ and $\mathbf{N}_{rotor}$ are the mass matrix, the damping matrix, the gyroscopic matrix, the stiffness matrix, the centrifugal stiffening matrix and the spin softening matrix, respectively. The vector $\mathbf{X}_{rotor}$ defining the generalised degrees of freedom vector of the system contains $2m_{tot} + 2 + n_{tot}N_{tot}$ elements and has the following expression:

$$\mathbf{X}_{rotor} = \left[U_0 \;\; V_0 \;\; U_1 \;\; V_1 \;\; \ldots \;\; U_{m_{tot}} \;\; V_{m_{tot}} \;\; X_{11} \;\; X_{21} \;\; \ldots \;\; X_{n_{tot}1} \;\; \ldots \;\; X_{1N_{tot}} \;\; \ldots \;\; X_{n_{tot}N_{tot}}\right]^T \quad (13)$$

Since the model has been fully developed in the rotating frame there are no time-dependent terms resulting from the periodicity of the rotating structure, in the analytical formulation and this is particularly useful to study such rotating structure. For instance, the eigenvalues and the stability of the flexible bladed rotor can be investigated by determining the solutions $\lambda = a + ib$ of the characteristic equation:

$$\det(\lambda^2\mathbf{M}_{rotor} + \lambda\tilde{\mathbf{C}}_{rotor} + \tilde{\mathbf{K}}_{rotor}) = 0 \quad (14)$$

where $\tilde{\mathbf{C}}_{rotor}$ and $\tilde{\mathbf{K}}_{rotor}$ are the generalised damping and stiffness matrices for the stator respectively. The rotor becomes unstable if any one or more of the eigenvalues' real part a is positive whereas the eigenvalues' imaginary parts correspond to the eigen frequencies of the system. So, the evolution of these eigenvalues' imaginary parts as a function of the rotational speed of the rotor give a Campbell diagram in the rotating frame. Figure 3(a) represents a Campbell diagram for a flexible twenty eight-bladed-rotor of one meter in length, supported by three isotropic bearings having radial stiffness and viscous damping coefficients of $k_{bearing}=2.10^7 N.m^{-1}$ and $D_{bearing} = 2.10^3 N.s.m^{-1}$. In the rotating frame, the negative slope curves are forward modes (precession motions in the same sense of rotation as the own rotation of the shaft) and the positive slope ones are backward modes. The evolutions of the shaft's eigen-frequencies, shown on Fig. 3(a), are mainly due to the gyroscopic effects. The evolution of the blades' eigen-frequencies (starting at 31 Hz) i.e. their stiffening, is due to the centrifugal effects included in the pre-stress potential v_{gblade}. Two loci separation phenomena (Pierre, 1988) can be seen as illustrated by the points A and B: when two eigenvalue loci approach each other, they either cross or do not cross; often in the latter case, even though the loci nearly intersect, in fact they do not but rather veer away from each other. Fig. 4 represents the mode shapes associated with the veering phenomenon *A*. Before this phenomenon, the mode shape associated with the lower frequency (among both concerned mode shapes) consists mainly in a shaft mode having one node (see Fig. 4(a)) and the one associated with the higher frequency consists also mainly in a shape mode but, having two nodes (see Fig. 4(b)). After the veering, the mode shape associated with the lower frequency consists in a shaft mode having two nodes (see Fig. 4(d)) where as the mode associated with the higher frequency consists in a shaft mode having one node (see Fig. 4(c)).During these veering phenomena, mode shapes and sense of rotation are switched between the eigenvalues that veer away from each other. Moreover, the stability of the system can be known by correlating these curves to these of the Fig. 3(b) representing the evolution of the eigenvalues' imaginary parts but as a function of the associated eigenvalues' real parts. In this case, it can be seen that the system is perfectly stable because there is no eigenvalues having a real part positive.Such stability analysis can be performed for several rotating systems and stability maps can also be obtained (Lesaffre et al., 2004).

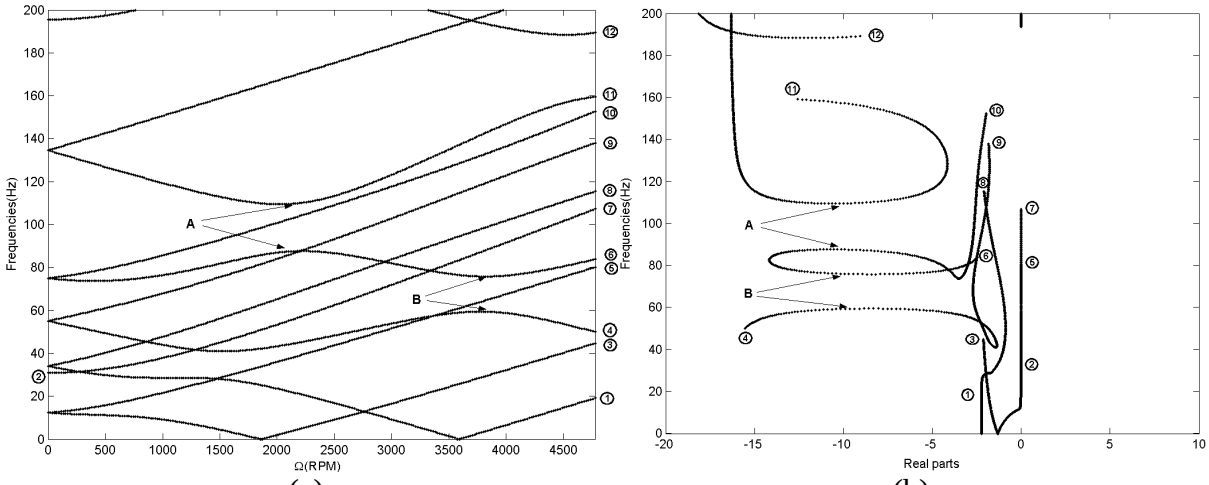

(a) (b)

Figure 3 (a) Campbell diagram (b) Complex plane diagram for a twenty eight-bladed-rotor with blades of one meter in length

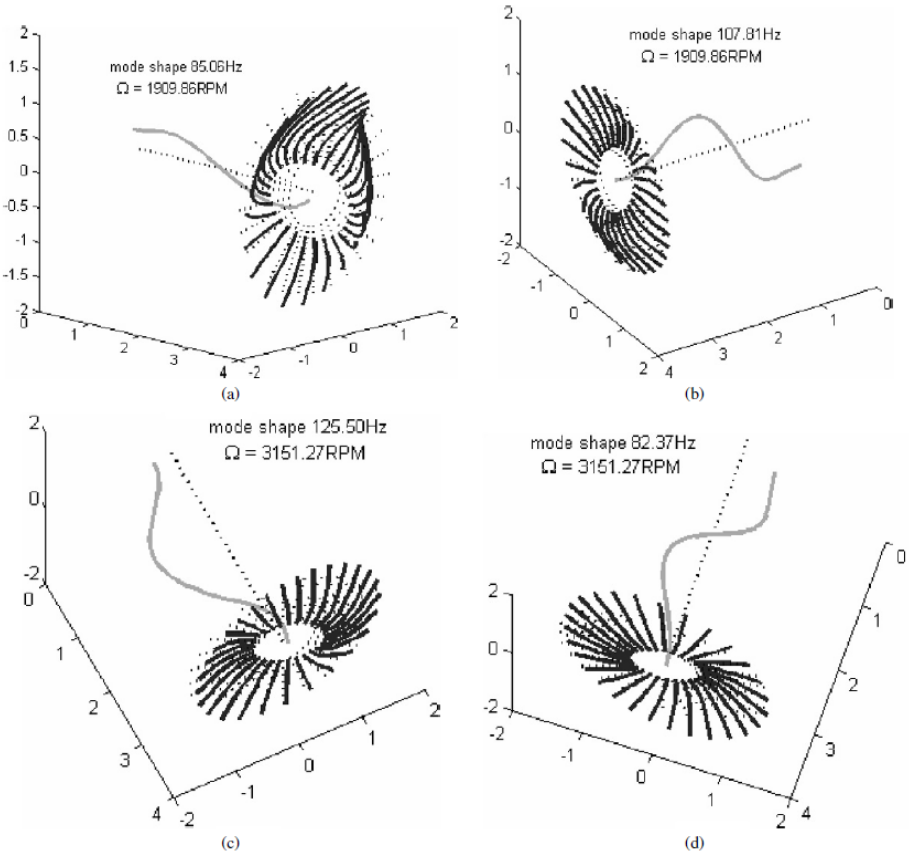

Fig. 4. Mode shapes of the rotor associated to the veering phenomenon A on Fig. 3, (a) and (b): before the veering, (c) and (d): after the veering.

III. Rotor-stator contact

a. Simple model of rotating loads on the elastic casing

Prior to the study of the contact between the blades of the rotor and the casing, a simple model of an elastic ring excited by rotating loads is developed in the rotating frame by using also an energetic method. This model consists in p loads, composed of a spring (with stiffness k_j) and a mass m_j located at the angles ϕ_j in the rotating frame, rotating permanently on an elastic stator without rubbing (Cf. Fig. 5b). The only radial degree of freedom of these spring-masses are thus the same as the radial displacements u_s of the ring at ϕ_j. Their kinetic energy and their potential energy are defined:

$$T_{loads} = \sum_{j=1}^{p} \frac{1}{2} m_j \left[\dot{u}_s^2(\phi,t) + \Omega^2 \left(R_{stat} - u_s(\phi,t) \right)^2 \right] \delta\left(\phi - \phi_j\right) \tag{15}$$

$$v_{loads} = \sum_{j=1}^{p} \frac{1}{2} k_j u_s^2(\phi,t) \delta\left(\phi - \phi_j\right) \tag{16}$$

The casing is modelled by a flexible circular beam (see Fig. 5a). The in-plane flexural vibrations of the ring are considered. Thus, two degrees of freedom are considered in the rotating frame: the radial displacement $u_s(\phi,t)$ and the tangential displacement $w(\phi,t)$ (see Fig. 5). This latter one can be expressed by (Love, 1944) :

$$w(\phi,t)=\sum_{n=2}^{k_{tot}} A_n(t)\cos n\phi + B_n(t)\sin n\phi \tag{17}$$

where the rigid body motion has been eliminated. The considered stator is supposed to be inextensible, implying thus that the radial displacement can be expressed from the tangential one by:

$$u_s(\phi,t)=\frac{\partial w(\phi,t)}{\partial \phi} \tag{18}$$

The stator is also fully described in the rotating frame. Its kinetic energy T_{stat}, as well as its potential energy v_{stat} are defined:

$$T_{stat}=\frac{1}{2}\int_{-\Omega t}^{2\pi-\Omega t}\rho_{stat}S_{stat}\left\{\left[\dot{u}_s(\phi,t)-\Omega\frac{\partial u_s}{\partial\phi}(\phi,t)\right]^2+\left[\dot{w}(\phi,t)-\Omega\frac{\partial w}{\partial\phi}(\phi,t)\right]^2\right\}R_{stat}d\phi \tag{19}$$

$$\gamma_{stat}=\frac{1}{2}\int_{-\Omega t}^{2\pi-\Omega t}\frac{E_{stat}I_{stat}}{R_{stat}^3}\left\{\frac{\partial^2 u_s}{\partial\phi^2}(\phi,t)+\frac{\partial w}{\partial\phi}(\phi,t)\right\}^2 d\phi \tag{20}$$

In these expressions, ρ_{stat}, S_{stat}, E_{stat} and I_{stat} are the density, the cross section area, the elastic Young's modulus of the ring material and the area moment of inertia for flexure of the casing respectively. It must be noted that the present ring is not damped. For simplicity reason, only one mode shape of the casing (the n^{th} one) is considered at a time thus the dynamic behaviour of the system is governed by a 2×2 matrix equation. The matrix equation of the dynamic behaviour of the ring excited by p rotating spring-masses, without rubbing, can be obtained by using Lagrange's equations and has the following expression:

$$\begin{bmatrix}\rho_{stat}S_{stat}R_{stat}\pi\left(n^2+1\right)+\sum_{j=1}^{p}m_j n^2\sin^2(n\phi_j) & -\sum_{j=1}^{p}m_j n^2\sin(n\phi_j)\cos(n\phi_j)\\ -\sum_{j=1}^{p}m_j n^2\sin(n\phi_j)\cos(n\phi_j) & \rho_{stat}S_{stat}R_{stat}\pi\left(n^2+1\right)+\sum_{j=1}^{p}m_j n^2\cos^2(n\phi_j)\end{bmatrix}\begin{Bmatrix}\ddot{A}_n\\ \ddot{B}_n\end{Bmatrix}$$
$$+\begin{bmatrix}0 & -2\pi\rho_{stat}S_{stat}R_{stat}n\Omega\left(n^2+1\right)\\ 2\pi\rho_{stat}S_{stat}R_{stat}n\Omega\left(n^2+1\right) & 0\end{bmatrix}\begin{Bmatrix}\dot{A}_n\\ \dot{B}_n\end{Bmatrix}$$
$$+\begin{bmatrix}\frac{E_{stat}I_{stat}\pi}{R_{stat}^3}n^2(n^2-1)^2-\rho_{stat}S_{stat}R_{stat}\pi n^2\Omega^2\left(n^2+1\right)+\sum_{j=1}^{p}(k_j-m_j\Omega^2)n^2\sin^2(n\phi_j) & -\sum_{j=1}^{p}(k_j-m_j\Omega^2)n^2\sin(n\phi_j)\cos(n\phi_j)\\ -\sum_{j=1}^{p}(k_j-m_j\Omega^2)n^2\sin(n\phi_j)\cos(n\phi_j) & \frac{E_{stat}I_{stat}\pi}{R_{stat}^3}n^2(n^2-1)^2-\rho_{stat}S_{stat}R_{stat}\pi n^2\Omega^2\left(n^2+1\right)+\sum_{j=1}^{p}(k_j-m_j\Omega^2)n^2\cos^2(n\phi_j)\end{bmatrix}\begin{Bmatrix}A_n\\ B_n\end{Bmatrix} \tag{21}$$
$$=\begin{Bmatrix}\sum_{j=1}^{p}m_j R_{stat}\Omega^2 n\sin(n\phi_j)\\ -\sum_{j=1}^{p}m_j R_{stat}\Omega^2 n\cos(n\phi_j)\end{Bmatrix}$$

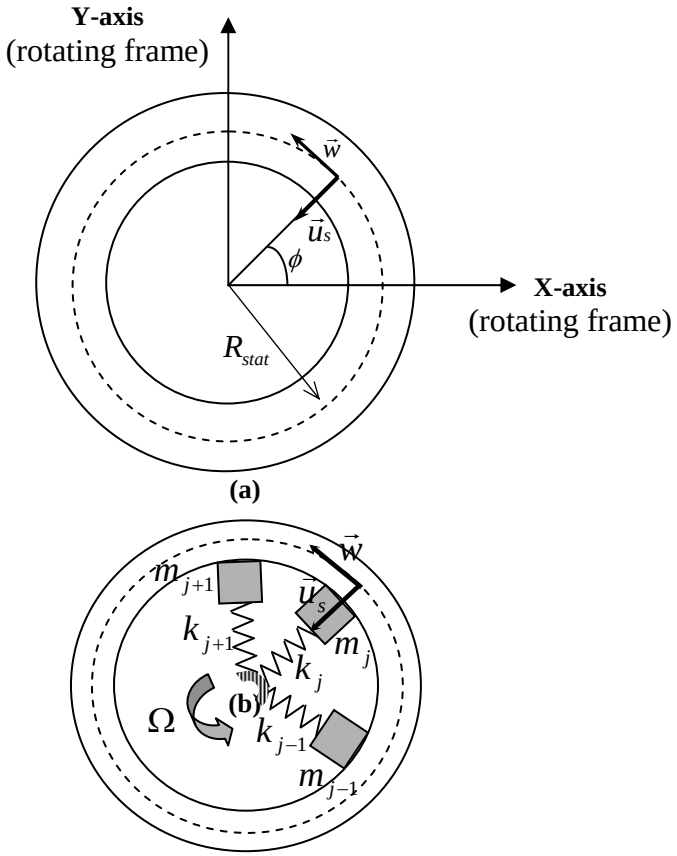

Figure 5 (a) Flexible casing, (b) model of moving loads on an elastic stator without rubbing

The stability of the casing can be studied by determining the eigenvalues of this matrix equation. The influence of the stiffness, of the mass and of the number of the moving loads can be studied. For instance, in the particular case of only one rotating radial spring-mass on the casing, the matrix equation of the dynamic behaviour of the system is the following one:

$$\begin{bmatrix} M_{stat}\left(n^2+1\right) & 0 \\ 0 & M_{stat}\left(n^2+1\right)+mn^2 \end{bmatrix}\begin{Bmatrix} \ddot{A}_n \\ \ddot{B}_n \end{Bmatrix} + \begin{bmatrix} 0 & -2M_{stat}n\Omega\left(n^2+1\right) \\ 2M_{stat}n\Omega\left(n^2+1\right) & 0 \end{bmatrix}\begin{Bmatrix} \dot{A}_n \\ \dot{B}_n \end{Bmatrix}$$
$$+\begin{bmatrix} K_{stat}n^2(n^2-1)^2 - M_{stat}n^2\Omega^2\left(n^2+1\right) & 0 \\ 0 & K_{stat}n^2(n^2-1)^2 - M_{stat}n^2\Omega^2\left(n^2+1\right)+(k-m\Omega^2)n^2 \end{bmatrix}\begin{Bmatrix} A_n \\ B_n \end{Bmatrix} = \begin{Bmatrix} 0 \\ -mR_{stat}\Omega^2 n \end{Bmatrix} \quad (22)$$

$$\text{with } M_{stat} = \rho_{stat} S_{stat} R_{stat} \pi \text{ and } K_{stat} = \frac{E_{stat} I_{stat} \pi}{R_{stat}^3}$$

It can be seem that the stiffness matrix can become singular and thus the system is likely to experience some unstable phenomenon (Crandall, 1995) as shown on Fig. 5 representing a stability analysis of the two nodal diameter mode shape of the stator excited by one rotating spring-mass.

Two kinds of instabilities appear: divergence (instability at zero frequency) of the forward mode shape and mode coupling (the forward and the backward mode shapes of the stator become two mode shapes having the same eigen-frequency but one of them being

stable and the other, unstable). The critical rotational speeds where the system diverges can be expressed analytically through the Routh-Hurwitz criterion applied to the characteristic polynom $\tilde{P}(x) = Ax^2 + Bx + C$ instead of $P(s) = As^4 + Bs^2 + C = \det\left(s^2\mathrm{M} + s\mathrm{G} + \mathrm{K}\right)$, in this simple case of only one rotating spring-mass (in the latter equation, **M**, **G** and **K** are the matrix written in Eq. 22). According to this criterion, the polynom $\tilde{P}(x) = Ax^2 + Bx + C$ has all its roots with real parts negative if A, B and C have the same sign. Thus, it turns out that :

- for a light mass i.e. $2M_{stat} > m$, with $M_{stat} = \pi\rho_{stat}S_{stat}R_{stat}$, the system can experience divergence if :

$$\Omega_c^2 < \Omega^2 < \Omega_{c2}^2 \tag{23}$$

with

$$\Omega_{c2}^2 = \frac{\Omega_c^2}{1+\dfrac{m}{M_{stat}\left(n^2+1\right)}} + \frac{\omega^2}{1+\dfrac{M_{stat}\left(n^2+1\right)}{m}} \tag{24}$$

and

$$\Omega_c^2 = \frac{E_{stat}I_{stat}}{\rho_{stat}S_{stat}R_{stat}^4}\frac{\left(n^2-1\right)^2}{n^2+1} = \frac{\omega_{stat_n}^2}{n^2} \tag{25}$$

in the case of $\omega^2 = \dfrac{k}{m} > \Omega_c^2$ or, if $\Omega_{c2}^2 < \Omega^2 < \Omega_c^2$ in the case of $\omega^2 < \Omega_c^2$.

- if the spring-mass has a heavy mass i.e. $2M_{stat} < m$, the system can also experience divergence if :

$$\Omega^2 > \Omega_{c3}^2 \tag{26}$$

with

$$\Omega_{c3}^2 = \Omega_c^2\left[\frac{2M_{stat}\left(n^2+1\right)+n^2m}{m\left(n^2+1\right)-2M_{stat}\left(n^2+1\right)}\right] + \frac{k}{m\left(n^2+1\right)-2M_{stat}\left(n^2+1\right)} \tag{27}$$

In these expressions, Ω_c is the wave propagation speed in the stator for its n^{th} mode shape and so, its n^{th} critical rotational speed in the rotating frame. Thus, it appears that both the mass and the stiffness of the spring-mass can make the system diverge. In a general manner, the bigger the stiffness is, the larger the speed range where the system can experience divergence is. For strong stiffness, this speed range begins at Ω_c and closes far away at Ω_{c2}. Concerning the mass, the heavier it is, the earlier the speed range where the system can experience divergence is. The critical speed where the system experiences mode coupling cannot be determined with the Routh-Hurwitz criterion as for the divergence instabilities (in the general case, the real part of $x = s^2$ is not the same as s). However, this critical speed can also be determined analytically in the particular case of only one rotating spring-mass. As a matter of fact, a sufficient condition for the apparition of flutter, in this particular case of an undamped structure, is to have two eigenvalues with real parts null and opposite imaginary parts. These conditions can be satisfied if the discriminant of $\tilde{P}(x)$ is null. Thus, the critical speed of mode coupling for the system satisfy $B^2 - 4AC = 0$. In the particular case of only one rotating spring-mass, the rotational speeds satisfying the latter equation can be expressed by :

$$\Omega_{mc} = \pm\frac{\left\{m\chi\left[\gamma \pm 4\sqrt{\xi}\right]\right\}^{1/2}}{mn\chi} \tag{28}$$

providing that the square roots can be defined, with:

$$\chi = \left[8M_{stat}\left(n^2+1\right)^2 - m\left(n^2-1\right)^2\right] \tag{29}$$

$$\gamma = 4M_{stat}\left(n^2+1\right)\left(2K_{stat}+n^2k\right)+mn^2\left(4K_{stat}+\left(n^2-1\right)\left[k-n^2m\Omega_c^2\right]\right) \quad (30)$$

$$\xi = \left(M_{stat}\left(n^2+1\right)+n^2m\right)\left(M_{stat}\left(n^2+1\right)\left[n^2k+2K_{stat}\right]^2+K_{stat}mn^2\left[mn^2\Omega_c^2-k\left(n^2+1\right)\right]\right) \quad (31)$$

$$K_{stat} = \frac{E_{stat}I_{stat}\pi}{R_{stat}^3}\left(n^3-n\right)^2 \quad (32)$$

The following figures illustrate these theoretical results. Figure 7 shows a stability analysis of the system in the case of a light mass $2M_{stat} > m$. Figure 7b shows that only the mass is responsible of mode couplings. Figures 7c and 7d show that the stiffness seems to move back the critical speed where mode couplings appear. Figure 8 shows also a stability analysis for the same system but in the case of a heavy mass $2M_{stat} < m$. It should have two speed ranges where the system diverges: the first one from Ω_{c2} to Ω_c, the second one being from $\Omega_{c3} = 403RPM$. However, this latter divergence cannot be seen on Fig. 8 because mode couplings occur before. Thus, this shows (with Fig. 7b and 7c) that the heavier the mass is, the earlier the system experiences mode couplings (at least in the mass range studied here).

The last parameter study considers the number of moving loads. Figures 9a, 9b, 9c and 9d represent the real parts and the eigen-frequencies of the two nodal diameter mode shape of the stator with respectively one, two, three moving loads separated from 60° to each others (like blades ①, ②, ③ on Fig. 11) and three moving loads, two separated from 180° and the third one at 60° from one of the latter two (like blades ①, ② and ④ on Fig. 11). These pictures have been made in the case of light masses $m = 10kg$ and stiffness $k = 1e7N.m^{-1}$. In a general case, the influence of the number of moving loads on the stability of the stator is not obvious. However, in some particular configurations of the moving loads in comparison to the mode shape considered, the divergence instability can disappear as shown on Fig. 8c. In our case and according to the Routh-Hurwitz criterion, a sufficient condition for the stator excited by several rotating loads with light masses ($2M_{stat} > \left[\sum_j m_j + \frac{2n^2\left(\sum_j m_j \sin^2(n\phi_j)\right)^2}{M_{stat}\left(n^2+1\right)^2}\right]$) to avoid divergence instability is:

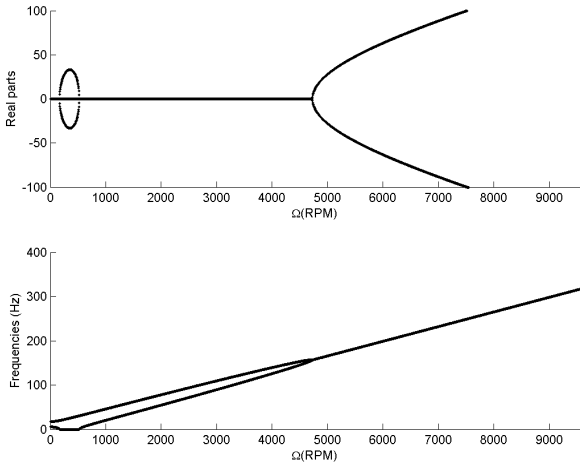

Figure 6 Stability analysis of the two nodal diameter mode shape of the stator excited by one rotating spring-mass with $m = 10kg$ and $k = 1e7N.m^{-1}$

$$\begin{cases} \sum_{j=1}^{p} k_j \sin^2(n\phi_j) = \sum_{j=1}^{p} k_j \cos^2(n\phi_j) \\ \sum_{j=1}^{p} k_j \sin(n\phi_j)\cos(n\phi_j) = 0 \\ \sum_{j=1}^{p} m_j \sin^2(n\phi_j) = \sum_{j=1}^{p} m_j \cos^2(n\phi_j) \\ \sum_{j=1}^{p} m_j \sin(n\phi_j)\cos(n\phi_j) = 0 \end{cases} \tag{33}$$

Thus, for instance, in the case shown on Fig. 9c, all the conditions are satisfied: the masses are light, all the stiffness and masses are the same and:

$$\begin{cases} \sin^2(2\frac{\pi}{6}) + \sin^2(2\frac{2\pi}{6}) + \sin^2(2\frac{3\pi}{6}) = \cos^2(2\frac{\pi}{6}) + \cos^2(2\frac{2\pi}{6}) + \cos^2(2\frac{3\pi}{6}) = \frac{3}{2} \\ \sin(2\frac{\pi}{6})\cos(2\frac{\pi}{6}) + \sin(2\frac{2\pi}{6})\cos(2\frac{2\pi}{6}) + \sin(2\frac{3\pi}{6})\cos(2\frac{3\pi}{6}) = 0 \end{cases} \tag{34}$$

what is not the case of the Fig. 9d:

$$\begin{cases} \sin^2(2\frac{\pi}{6}) + \sin^2(2\frac{2\pi}{6}) + \sin^2(2\frac{4\pi}{6}) = \frac{9}{4} \\ \cos^2(2\frac{\pi}{6}) + \cos^2(2\frac{2\pi}{6}) + \cos^2(2\frac{4\pi}{6}) = \frac{3}{4} \\ \sin(2\frac{\pi}{6})\cos(2\frac{\pi}{6}) + \sin(2\frac{2\pi}{6})\cos(2\frac{2\pi}{6}) + \sin(2\frac{4\pi}{6})\cos(2\frac{4\pi}{6}) = \frac{\sqrt{3}}{4} \neq 0 \end{cases} \tag{35}$$

The Routh-Hurwitz criterion shows also that if $2M_{stat} < \left[\sum_j m_j + \frac{2n^2 \left(\sum_j m_j \sin^2(n\phi_j) \right)^2}{M_{stat}\left(n^2+1\right)^2} \right]$ then, the system can experience divergence for :

$$\Omega^2 > \Omega_c^2 \left[\frac{2M_{stat}\left(n^2+1\right) + n^2 \sum_j m_j}{\left(n^2+1\right)\sum_j m_j + \frac{2n^2 \left(\sum_j m_j \sin^2(n\phi_j) \right)^2}{M_{stat}\left(n^2+1\right)} - 2M_{stat}\left(n^2+1\right)} \right] + \frac{M_{stat}\left(n^2+1\right)\sum_j k_j + 2n^2 \left[\sum_j k_j \sin^2(n\phi_j) \right] \left[\sum_j m_j \sin^2(n\phi_j) \right]}{M_{stat}\left(n^2+1\right)^2 \left[\sum_j m_j + \frac{2n^2 \left(\sum_j m_j \sin^2(n\phi_j) \right)^2}{M_{stat}\left(n^2+1\right)^2} - 2M_{stat} \right]} \tag{36}$$

Figure 10 shows the same stability analysis as Fig. 8c but with three masses of $1000kg$. The system would have experience divergence from $\Omega > 786RPM$ but since it has be seen that the heavier the mass is, the earlier the system experiences mode couplings, the system is unstable from $\Omega > 622RPM$ but does not diverge.

Since some phenomenon occurring when an elastic structure is excited by rotating loads have been analysed and understood, the study of the contact between the blades of the rotor and the flexible casing of a turbo-machine can be performed.

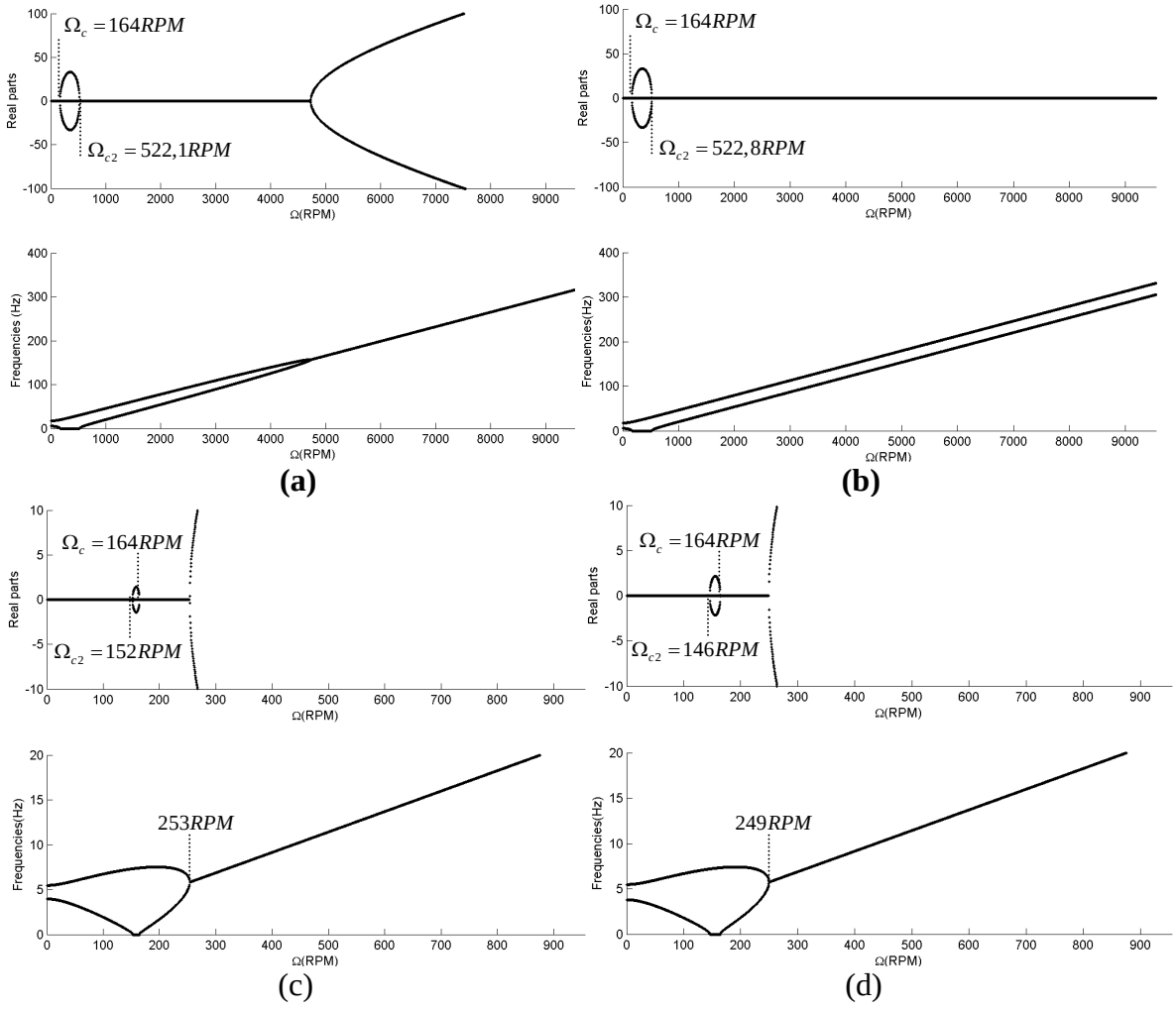

Figure 7 Stability analysis of the two nodal diameter mode shape of the stator excited by one rotating spring-mass with $2M_{stat} > m$ a) $k = 1e7N.m^{-1}$, $m = 10kg$ ($\omega = 9550RPM > 164RPM = \Omega_c$), b) $k = 1e7N.m^{-1}$, $m = 0kg$, c) $k = 1e5N.m^{-1}$, $m = 1000kg$ ($\omega = 95,5RPM < 164RPM = \Omega_c$), d) $k = 0N.m^{-1}$, $m = 1000kg$

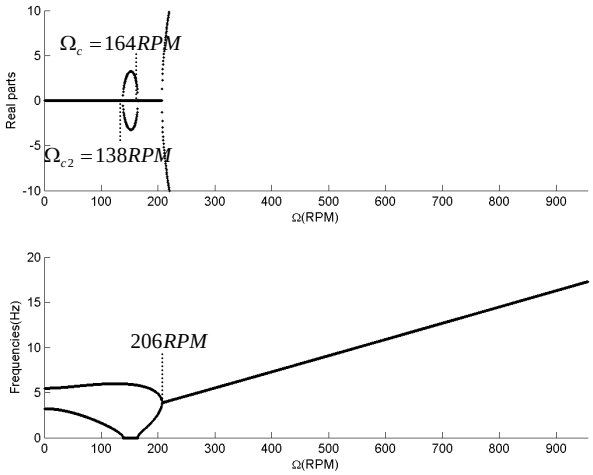

Figure 8 Stability analysis of the two nodal diameter mode shape of the stator excited by one rotating spring-mass with $m = 2000kg$ ($m > 2M_{stat}$) and $k = 1e5N.m^{-1}$

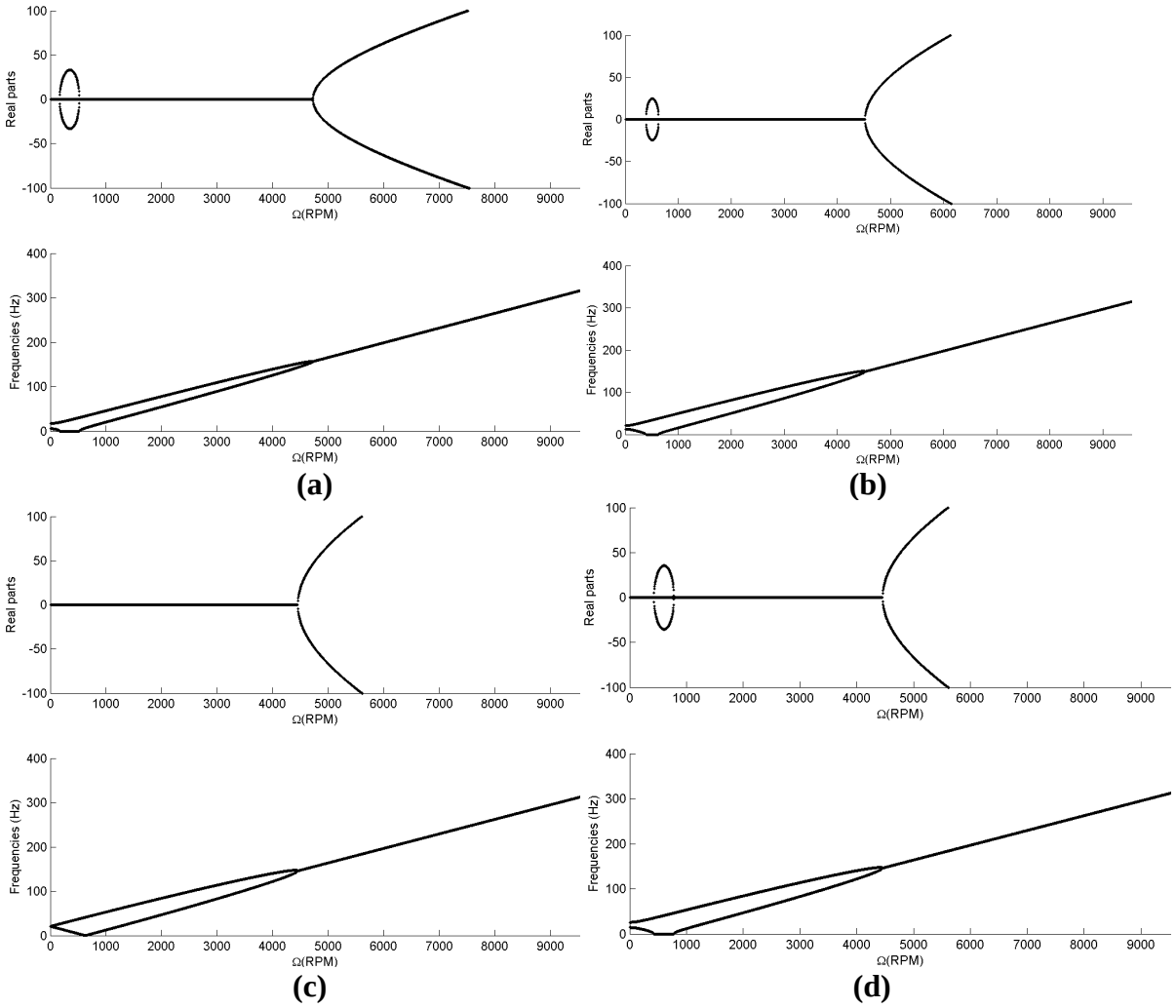

Figure 9 Influence of the number of moving loads on the two nodal diameter mode shape of the stator with a) one moving load b) two moving loads in a configuration like blades ① and ② c) three moving loads in configuration like blades ①, ② and ③ and d) with three moving loads in configuration like blades ①, ② and ④

b. Blade tips/Casing Contact

The contact between the flexible blade tips and a flexible casing is introduced by assuming no rubbing between the two structures.

In this section, the casing considered is the same as in the latter section but with internal viscous damping (with coefficient η_{stat}) introduced through a function of dissipation F_{dstat}:

$$F_{d_{stat}} = \frac{1}{2}\int_{-\Omega t}^{2\pi-\Omega t} \eta_{stat}\frac{E_{stat}I_{stat}}{R_{stat}^3}\left\{-\Omega\frac{\partial^3 u_s}{\partial\phi^3}(\phi,t)+\frac{\partial^2 \dot{u}_s}{\partial\phi^2}(\phi,t)-\Omega\frac{\partial^2 w}{\partial\phi^2}(\phi,t)+\frac{\partial \dot{w}}{\partial\phi}(\phi,t)\right\}^2 d\phi \tag{37}$$

and with more than one mode shape considered. If k_{tot} modes shapes are considered to express the ring displacements, its dynamic behaviour in the rotating frame can be described, as for the rotor, by a set of equations that can be written under the following form:

$$\mathbf{M}_{stat}\ddot{\mathbf{X}}_{stat}+\tilde{\mathbf{C}}_{stat}\dot{\mathbf{X}}_{stat}+\tilde{\mathbf{K}}_{stat}\mathbf{X}_{stat}=\mathbf{0} \tag{38}$$

where $\mathbf{M}_{stat}$, $\tilde{\mathbf{C}}_{stat}$ and $\tilde{\mathbf{K}}_{stat}$ are the mass matrix, the generalised damping matrix, including the gyroscopic matrix, and the generalised stiffness matrix, including the spin softening matrix, for the stator respectively. The vector $\mathbf{X}_{stat}$ which defines the generalised degrees of freedom vector of the stator contains $2k_{tot}-2$ elements and has the following expression: $\mathbf{X}_{stat}=\left[A_2 \quad B_2 \quad . \quad . \quad . \quad A_{k_{tot}} \quad B_{k_{tot}}\right]^T$.

The contact problem is treated by using Lagrangian multipliers λ_j. A contact energy E_{λ_j} is defined for each contact at the j^{th} blade located at the angle φ_j in the rotating frame:

$$E_{\lambda_j}=\lambda_j\left(u(l,t)\cos\varphi_j+\upsilon(l,t)\sin\varphi_j+u_s(\phi=\varphi_j,t)-clearance\right) \tag{39}$$

This energy is proportional to a Lagrangian multiplier (one per contact) and to the clearance between the blade tip and the casing. Thus there is one more equation per contact and also one more second member per contact in the behaviour equation of the system. Since the contact energy depends also on the radial displacement of the ring, the degrees of freedom of both structures are coupled. The contact between the rotor and the casing is supposed to be due to an unbalance strength. The dynamic behaviour of the whole structure can be described through the following matrix equation:

$$\begin{bmatrix}\mathbf{M}_{rotor} & \mathbf{0} & \\ & \mathbf{0} & \mathbf{M}_{stator}\end{bmatrix}\begin{Bmatrix}\ddot{\mathbf{X}}_{rotor}\\ \ddot{\boldsymbol{\lambda}}\\ \ddot{\mathbf{X}}_{stator}\end{Bmatrix}+\begin{bmatrix}\tilde{\mathbf{C}}_{rotor} & \mathbf{0} & \\ & \mathbf{0} & \tilde{\mathbf{C}}_{stator}\end{bmatrix}\begin{Bmatrix}\dot{\mathbf{X}}_{rotor}\\ \dot{\boldsymbol{\lambda}}\\ \dot{\mathbf{X}}_{stator}\end{Bmatrix}+\begin{bmatrix}\tilde{\mathbf{K}}_{rotor} & \mathbf{0} & \\ & \mathbf{0} & \tilde{\mathbf{K}}_{stator}\end{bmatrix}\begin{Bmatrix}\mathbf{X}_{rotor}\\ \boldsymbol{\lambda}\\ \mathbf{X}_{stator}\end{Bmatrix}=\begin{Bmatrix}\mathbf{F}_{unbalance}\\ \mathbf{F}_{\lambda}\\ \mathbf{0}\end{Bmatrix} \tag{40}$$

The rotational speed where the first contact appears has been placed under both the critical rotational speed of the rotor and of the stator by increasing the unbalance mass. In the rotating frame, this non linear problem is a static one. The balanced static contact configurations of the system are found by iterations: the first configuration of the rotor is found by resolving:

$$\tilde{\mathbf{K}}_{rotor}\mathbf{X}_{rotor}=\mathbf{F}_{unbalance} \tag{41}$$

If the clearance is consumed, the contact blades/casing exists and a new balanced static position is calculated by resolving the static part of Eq. 40:

$$\begin{bmatrix}\tilde{\mathbf{K}}_{rotor} & \mathbf{0} & \\ & \mathbf{0} & \tilde{\mathbf{K}}_{stator}\end{bmatrix}\begin{Bmatrix}\mathbf{X}_{rotor}\\ \boldsymbol{\lambda}\\ \mathbf{X}_{stator}\end{Bmatrix}=\begin{Bmatrix}\mathbf{F}_{unbalance}\\ \mathbf{F}_{\lambda}\\ \mathbf{0}\end{Bmatrix} \tag{42}$$

This non linear system has several balanced contact configurations and the evolution of the load acting on the system will influence the balanced configuration adopted. Thus, by increasing the rotational speed of the rotor, the evolution of the clearance between each blade tip and the casing can be followed as a function of the its rotational speed as shown in Fig. 12, in the particular case of a rotor having six blades (see Fig. 11). It can be seen that the first blade to touch the casing is the blade ①, then successively the blades ⑥, ② and ⑤, when the rotational speed increases. The associated deformed shape, at 164 RPM, is plotted on Fig. 13(a). When the rotational speed increases again, the blade ③ touches the stator. Thus, all the blades are in contact with the casing apart from the blade ④. The deformed shape associated, at 286 RPM, is plotted on Fig. 13(b). The system keeps this configuration while the rotational speed increases, until 310 RPM corresponding actually to the three nodal diameter mode shape critical speed of the casing. The associated deformed shape, at 310 RPM, is plotted on

Fig. 13(c). From this point, the algorithm diverges. It appears that up to this rotational speed, all the balanced static contact configurations found are stable ones but after this speed, the system has only unstable balanced static contact configurations. Moreover, from about 700 RPM, the system has no longer balanced static contact configurations. Figure 14 shows a synthesis of these three rotational speed ranges. It could have been thought that between 310 RPM and 700 RPM, the system might have stable dynamic contact configurations but, all the time integrations performed diverged on the three nodal diameter mode shape of the casing. This phenomenon can be explained by using the simple model of rotating loads on an elastic structure studied in the previous section.

Effectively, it has been shown that an elastic ring excited by rotating loads could experience two kind of instabilities: divergence instabilities and mode couplings. In order to know if the divergence of the rotor coupled with the flexible casing is due to this phenomenon, the latter model of rotating loads on the elastic ring can be used. To compare the results of both models, the loads exciting the ring must have the same modal parameters than the rotor hence, its modal parameters have to be evaluated. For simplicity, this will be done at $\Omega = 0 RPM$. If the rotor is submitted to a constant strength, its first modal mass an modal stiffness can be expressed by: $m_1 = \tilde{X}_1^T M_{rotor} X_1$ and $k_1 = \tilde{X}_1^T K_{rotor} X_1$, X_1 being its first eigen vector and $\tilde{X}_1$, its first eigen vector normalized so that the displacement of the rotor at the point of application of the strength and in its direction could be unity. The modal parameters for the rotor estimated like this are $m_1 = 4,45.10^4 kg$ and $k_1 = 6.23.10^{12} N.m^{-1}$. The latest stable balanced contact configuration (i.e. just before the system diverges) obtained statically and by time integration consists in five contacts: at blades ①, ②, ③, ⑤, and ⑥. Figures 15a and b represent the comparison between respectively the results (real parts and eigen-frequencies) obtained with the three nodal diameter mode shape of the simplified model having five moving loads configured like blades ①, ②, ③, ⑤, and ⑥ with m_1 and k_1 as parameters and, the Campbell diagram and the associated decay rate plot for the flexible casing in contact at blades ①, ②, ③, ⑤ and ⑥. The importance as well as the influence of the others mode shapes of the stator on each others appears through all the others instabilities that can be seen on Fig. 15b and not on Fig. 15a. However, these figures confirm that the stator experiences divergence through its three nodal diameter mode shape just after 310 RPM which is the critical speed Ω_c of this mode shape. So it can be said now that the instability of the three nodal diameter mode shape of the stator results from rotating loads on this elastic structure. Moreover, with this configuration of rotor i.e. with six blades separated by 60° from each others, there is no contact configuration that satisfies the four conditions to avoid the divergence of the three nodal diameter of the stator. Thus, until the dynamics of the blades is not introduced during contact i.e. until the balanced contact configurations consist in steady state contact, the blades will act as rotating loads on the stator and this one will always experience divergence on its three nodal diameter mode shape.

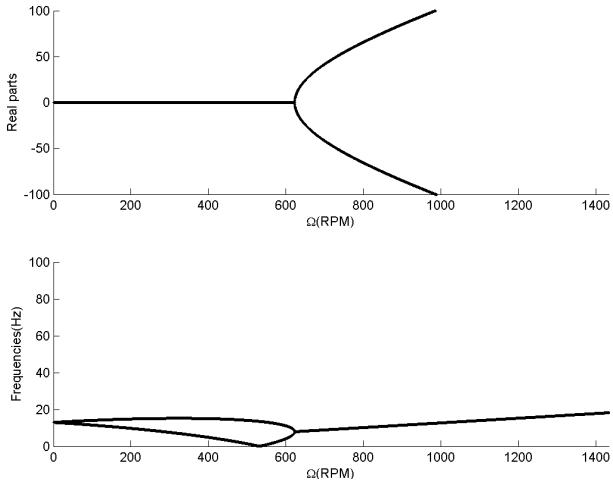

Figure 10 Stability analysis for the same system as shown by Fig. 8c but with masses of $1000kg$

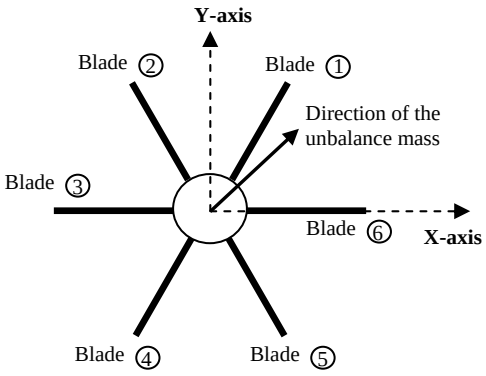

Figure 11 Blade numbers of a six bladed-rotor

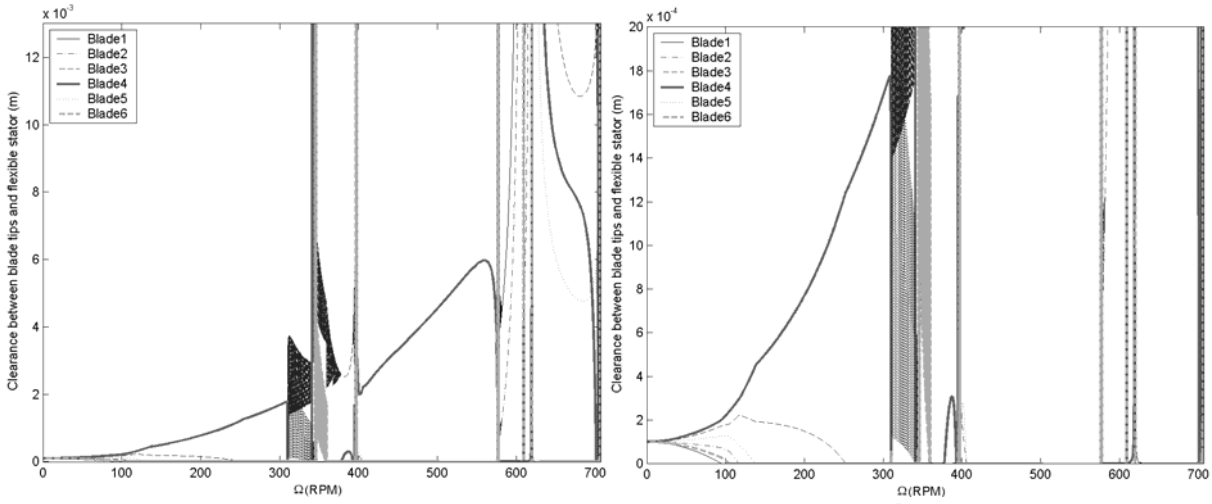

(a) (b)

Figure 12 (a) Evolution of the clearances between the blade tips and the flexible stator (b) zoom

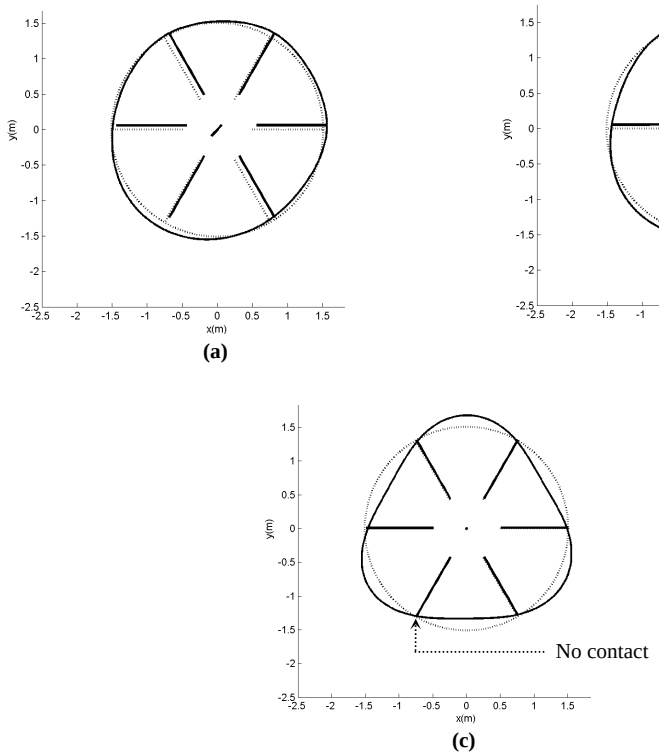

Figure 13 Contact configuration with a flexible casing at a) 164 RPM, b) 286 RPM and c) 310 RPM

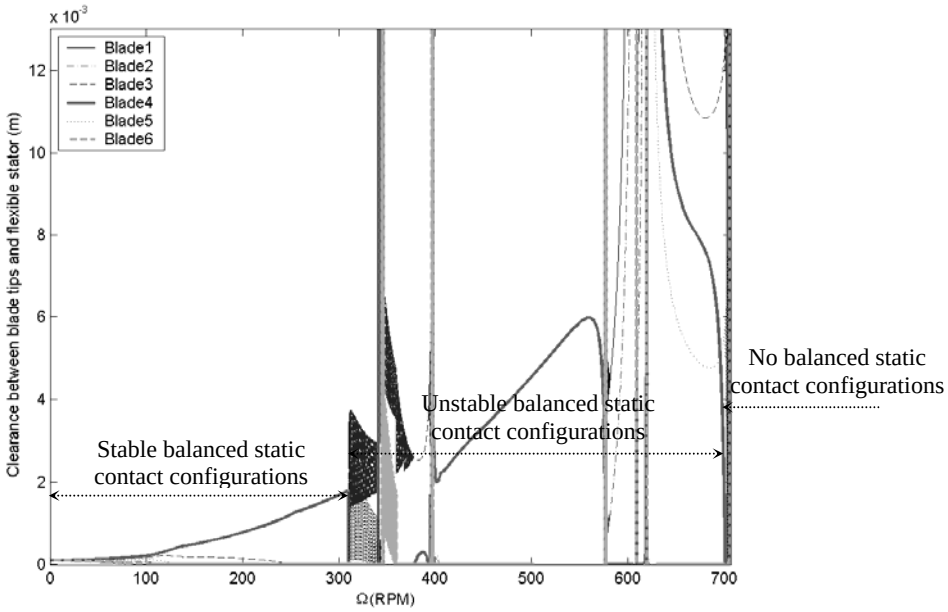

Figure 14 Rotational speed ranges for the evolution of the system

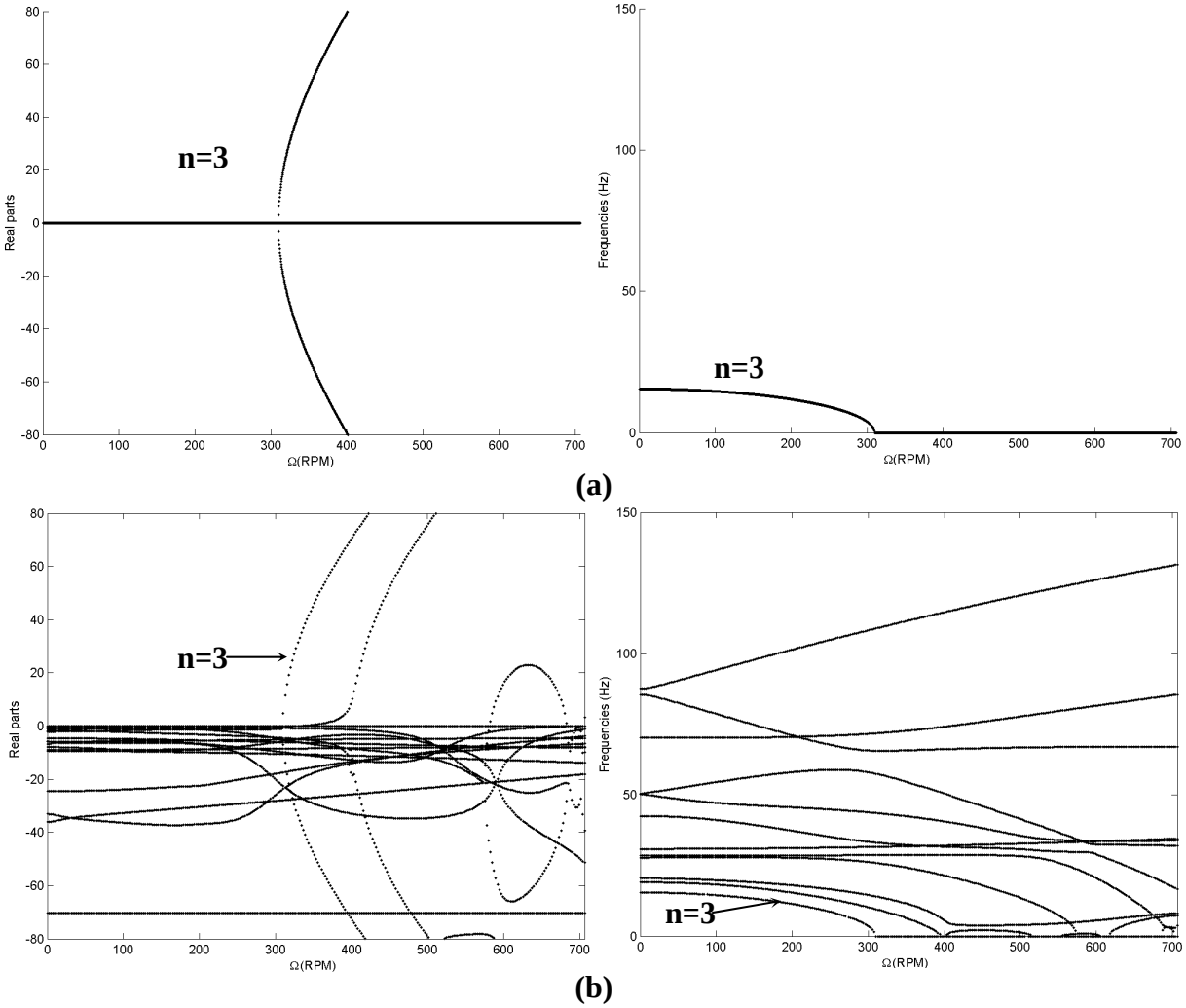

Figure 15 Comparison of real parts and eigen-frequencies between a) the three nodal diameter mode shape of the stator excited by five rotating loads angularly set like blades ①, ②, ③, ⑤ and ⑥ and whose parameters are m_1 and k_1 and b) the stator excited by the blades ①, ②, ③, ⑤ and ⑥

Conclusion

A flexible fully bladed-rotor has been modelled in the rotating frame using an energetic approach. The gyroscopic effects, the spin softening effects and the centrifugal stiffening effects have been taken into account so from a phenomenological point of view the system is almost complete. Moreover, the formulation obtained in the rotating frame appears to be useful to study such rotating structures, especially in case of contacts between the flexible blades and the casing. This very important problem has been first studied through a simple model of an elastic ring having only one mode shape and excited by rotating loads. This study has underlined that the considered structure can experience two kinds of instabilities: divergence instabilities and mode couplings. The influences of the loads' parameters have been analysed and in some simple cases, the critical speeds associated have been determined

analytically. Then, the casing of a turbo-machine has been modelled by an elastic ring too and the contact between the rotor of the machine and this casing has been studied. This problem has been solved, in part, by calculating the succession of the balanced static contact configurations of the system during an increase in its rotational speed, by using a Lagrangian multipliers method. It turns out that in the particular case of the rotor considered in this study, the system has several balanced configurations and adopts stable static configurations as a function of its rotational speed until the three nodal diameter mode shape critical speed of the casing where it always diverges. From this rotational speed, the system has neither stable balanced static contact configurations nor stable dynamic contact configurations. The latter simple model of an elastic ring excited by rotating loads used with the same parameters as the rotor has shown that this phenomenon results indeed from the action of the blades of the rotor acting like rotating loads on the casing.

References

Al-Bedoor, B.O., Al-Qaisia, A. A., 2005. “Stability Analysis of Rotating Blade Bending Vibration Due to Torsional Excitation”. Journal of Sound and Vibration, 282(3-5), pp. 1065-1083.

Arnoult, E, 1998. “Modelisation Numerique et Approche Experimentale du Contact en Dynamique: Application au Contact Aubes/Carter de Turboreacteur”. Ecole Centrale de Nantes. Thesis.

Childs, D., 1993. *Turbomachinery Rotordynamics: Phenomena, Modelling and Analysis*. John Wiley & Sons, Inc.

Crandall, S. H., Dugundji, J., 1981. “Resonant Whirling of Aircraft Propeller-Engine Systems”. Journal of Applied Mechanics, 48, pp. 929-935.

Crandall, S. H., 1995. “Rotordynamics”, in W. Kliemann and N. S. Namachchivaya, eds., Nonlinear Dynamics and Stochastic Mechanics, CRC Press, Boca Raton, pp. 1-44.

Edwards, S., Lees, A. W., Friswell, M. I., 1999. “The Influence of Torsion on Rotor/Stator Contact in Rotating Machinery”. Journal of Sound and Vibration, 225(4), pp. 767-778.

Ehrich, F. F., 1992. *Handbook of Rotordynamics*. Macgraw-Hill.

Ehrich, F. F., 1993. “Rotor Whirl Forces Induced by the Tip Clearance Effect in Axial Flow Compressors”. Journal of Vibration and Acoustics, 115, pp.509-515.

Feng, Z.C., Zhang, X-Z., 2002. “Rubbing Phenomena in Rotor-Stator Contact”. Chaos Solitons & Fractals, 14, pp. 257-267.

Genta, G., 2003. “On the Stability of Rotating Blade Array”. Journal of Sound and Vibration, 273, pp. 805-836.

Gmür, T., 1997. *Dynamique des structures*. Presses Polytechniques et universitaires romandes.

Goldman, P., Muszynska, A., 1995. “Rotor-to-Stator, Rub-related, Thermal/Mechanical Effects in Rotating Machinery”. Chaos Solitons & Fractals, 5(9), pp. 1579-1601.

Lalanne, M., Ferraris, G., 1990. *Rotordynamics Prediction in Engineering*. John Wiley & Sons.

Legrand, M., 2005. “ Modèles de prédiction de l'interaction rotor-stator dans un moteur d'avion”. Ecole Centrale de Nantes. Thesis.

Lesaffre, N., Sinou, J-J. and Thouverez, F. “Model and Stability Analysis of a Flexible Bladed-Rotor”. International Journal of Rotating Machinery. In Press.

Lesaffre, N., Sinou, J-J. and Thouverez, F., 2004. “Stability Analysis of a Flexible Blade-Rotor”. Key Engineering Materials, 292-294, pp. 409-416.

Love, A. E. H., 1944. *A Treatise on The Mathematical Theory of Elasticity*. New York Dover Publications.

Maozhong, Y., Baiyun, H., Jiawen, H., 2002. “Erosion Wear Behaviour and Model of Abradable Seal Coating”. Wear, 252, pp. 9-15.

Marscher, W. D., 1980. “A Phenomenological Model of Abradable Wear in High Performance Turbomachinery”. Wear, 59, pp. 191-211.

Muszynska, A., Bently, D., 1996. “Fluid-induced Instabilities of Rotors: Whirl and Whip – Summary of Results”. Orbit, pp.7-15.

Pierre, C., 1988. “Mode Localization and Eigenvalue Loci Veering Phenomena in Disordered Structures”. Journal of Sound and Vibration, 126(3), pp. 485-502.

Schmiechen, P., 1997. “Travelling Wave Speed Coincidence”. Imperial College of Science, Technology and Medicine, University of London. Thesis.

Sinha, S. K., 2004. “Dynamic Characteristics of a Flexible Bladed-rotor with Coulomb Damping Due to Tip-rub”. Journal of Sound and Vibration, 273, pp. 875-919.

Song, S. J., Martinez-Sanchez, M., 1997-a. “Rotordynamic Forces Due to Turbine Tip Leakage: part I- Blade Scale Effects”. Journal of Turbomachinery, 119, pp. 695-703.

Song, S. J., Martinez-Sanchez, M., 1997-b. “Rotordynamic Forces Due to Turbine Tip Leakage: part II- Radius Scale Effects and Experimental Verification”. Journal of Turbomachinery, 119, pp. 704-713.

Turhan, Ö., Bulut, G., 2005. “Dynamic Stability of Rotating Blades (Beams) Eccentrically Clamped to a Shaft with Fluctuating Speed”. Journal of Sound and Vibration, 280(3-5), pp. 945-964.

Yamamoto, T., Ishida, Y., 2001. *Linear and Nonlinear Rotordynamics: a Modern Treatment with Applications.* John Wiley & Sons.